Soft Matter

Dynamic Article Links

Cite this: *Soft Matter*, 2011, **7**, 11334

www.rsc.org/softmatter

PAPER

Structural forces in soft matter systems: unique flocculation pathways between deformable droplets

Rico F. Tabor,†[ab] Hannah Lockie,†[ab] Derek Y. C. Chan,[bcd] Franz Grieser,[be] Isabelle Grillo,[f] Kevin J. Mutch[g] and Raymond R. Dagastine*[ab]

Received 14th July 2011, Accepted 12th September 2011
DOI: 10.1039/c1sm06326j

Oscillatory structural forces caused by colloidal additives including micelles, microemulsion droplets and particles were explored between rigid and deformable interfaces using direct force measurements with the atomic force microscope. The observed oscillations from rigid surfaces become distorted when confinement occurs between deformable interfaces, giving rise to a force hysteresis between approaching and separating interfaces. Small-angle neutron scattering was used to determine the bulk structure of the colloidal additives, as a basis for comparison with their behaviour when confined in thin films. It is seen that confinement itself does not appear to significantly alter the structure of the colloidal additive when compared to the bulk; however, at small separations, interactions with the confining interfaces may become important. The combined approach uncovered an unique flocculation pathway that is available to deformable emulsion droplets, and that the strength of this flocculation can be tuned by changes in the size and concentration of the structuring colloid, the emulsion droplet size, and the ionic strength of the solution.

1 Introduction

A wide range of processes and products contain mixtures of colloidal additives of disparate sizes that are crucial to imparting the desired properties of the formulation. When these sizes are significantly different, for example, micron-scale emulsion droplets or particles in a solution containing nanoparticles, micelles or polymer coils, interesting behaviour emerges.[1] When present at low volume fractions, the smaller colloid may be responsible for the well-known depletion interaction,[2] which acts to flocculate objects by an osmotic attraction.[3] At higher concentrations, structural forces emerge, where the confinement of the smaller colloid in the thin films created by approaching interfaces causes oscillations in the force of interaction between the larger objects.[1,4]

These forces have been the subject of a great deal of interest and research, with papers detailing the effects of micelles,[5–8] particles,[9–11] polymer coils[4,11,12] and even solvent molecules confined between solid surfaces.[13] Due to the need to measure both force/pressure and separation, the techniques thus far used to measure these forces have involved the atomic force microscope (AFM)[6,9,10] surface forces apparatus (SFA),[13] total internal reflection microscope (TIRM)[4,7] and film drainage techniques.[5,14]

An important question that underlies the understanding of structural forces concerns whether the behaviour in the confining film is representative of that in the bulk, or whether the confinement itself causes perturbations. Several authors have attempted to correlate the nearest neighbour distance in the bulk with the distance between layers (or characteristic wavelength) from film measurements, where analyses based on the assumption of different packing arrangements suggest that the ordering of the smaller species within the film differs from that in the bulk.[9,15] Recent measurements of average inter-particle distance in bulk samples obtained from small-angle neutron scattering (SANS) and small-angle X-ray scattering (SAXS), appear to show that these values approximately correspond to layer distances in the film, and to values obtained from density functional theory (DFT) and Monte Carlo (MC) simulations.[10,16] This is indicative of the oscillations being due solely to bulk structuring under confined conditions down to the last oscillation. Further support of the solution maintaining bulk structure down to a very thin film is the finding that altering in surface potential induces only a change in the amplitude of the oscillations, with no change in the period.[17]

[a]*Department of Chemical and Biomolecular Engineering, University of Melbourne, Parkville, 3010, Australia. E-mail: rrd@unimelb.edu.au; Fax: +(61) 3 8344 4153; Tel: +(61) 3 8344 4704*
[b]*Particulate Fluids Processing Centre, University of Melbourne, Parkville, 3010, Australia*
[c]*Department of Mathematics and Statistics, University of Melbourne, Parkville, 3010, Australia*
[d]*Faculty of Life and Social Sciences, Swinburne University of Technology, Hawthorn, 3122, Australia*
[e]*School of Chemistry, University of Melbourne, Parkville, 3010, Australia*
[f]*Institut Max Von Laue Paul Langevin, F-38042 Grenoble, France*
[g]*Heinrich Heine University, Düsseldorf, D-40225, Germany*
† These authors contributed equally to this work.

At very small separations (around the oscillation at closest approach), some deviation is often seen between theory and experiment,[10,18] which is particularly marked at high concentrations. It has been suggested that this could be due to interactions of the structuring colloid with the interface, or due to an increase in density as film thickness is reduced.[10] However, such deviations have not yet been fully explained for solid systems. Conversely, in many deformable systems, it has been demonstrated that the capacity for enlargement of the interaction area rather than film thinning makes expulsion of this final layer of the structured film mechanically impossible.[19]

Structural forces between deformable interfaces, which are of relevance to emulsions and foams, have received less attention, most likely due to the added experimental challenges presented by their measurement and interpretation when compared to the solid case.[1,5,14,20] In film balance and film drainage experiments where large, planar interfaces are studied, interesting behaviour such as stratification and dimpling is observed.[18,20] However, these systems show minimal curvature and film pressures at least an order of magnitude lower than the Laplace pressure of a typical emulsified drop, potentially limiting their relevance to emulsion systems. In previous work, we demonstrated that structural forces could be observed between individual pairs of emulsion droplets, and that these forces were different depending on whether the droplets were approaching towards, or parting from, one another.[19] Gromer *et al.* noted similar hysteresis in the force between oil droplets when a polymer depletant was added.[21] Recent AFM measurements between an air bubble and a silica particle showed structuring effects in the presence of colloidal nanoparticles, but did not observe any hysteretic effects.[22]

When the disjoining pressure profile of a liquid film trapped between deformable interfaces shows a repulsive maximum accompanied by a retractive minimum, Bhatt *et al.* showed that this could give rise to a hysteretic behaviour in the measured force-displacement behaviour.[23] This is due to mechanical instabilities associated with the coupling of deformations of the deformable body and the cantilever, that can cause jumps to the next stable film thickness. We showed that the oscillating disjoining pressure profiles provided by structural interactions could indeed cause multiple hysteretic jumps in the AFM force-displacement data obtained from droplet systems.[19] It was seen that the oscillatory structural disjoining pressure when coupled to the deformable droplet interfaces was responsible for this behaviour, and significantly, that these effects could be predicted by using the measured pressure due to structural forces in a solid system.

In this work, we explore the effects of structural forces in rigid and deformable systems further:

- The structural effects of nanocolloidal additives between rigid surfaces are measured with AFM, in order to determine the disjoining pressure caused by their presence (section 3.1, Fig. 1)
- Structural forces between deformable oil/water interfaces are measured, to demonstrate the effects of the size and concentration of the structuring colloid, showing that the hysteresis in force behaviour only occurs for certain sized colloids (section 3.2, Fig. 2 and 3)
- Using theoretical modelling, it is shown that the hysteretic force behaviour is also controlled by the deformability of the confining interfaces, and hence for emulsion droplets, size and interfacial tension are the governing parameters (section 3.3, Fig. 4 and 5)
- Small-angle neutron scattering is employed to determine the bulk structure of the colloidal additives, and this is compared to structure in the film determined from AFM experiments, showing little difference between bulk and confined structure (section 3.4, Fig. 6, 7 and 8 and Table 1)
- To further explore the relationship between bulk structuring of the colloidal additives and their effects when confined in films between deformable objects, systems are explored at different ionic strengths, which emphasises the sensitivity of deformable interfaces to subtle changes in structural disjoining pressures. (section 3.5, Fig. 9 and 10)

2 Materials and methods

2.1 Materials

Sodium dodecyl sulfate (SDS) was obtained from Sigma (Ultra grade, 99%) and used as received. Perfluorooctane (PFO, 98%) and tetradecane (TD, 99%) were obtained from Aldrich and each purified by column chromatography over silica (Florisil, Sigma, 100–200 mesh). Deionised water was from a Milli-Q system, minimum resistivity 18.4 MΩ cm. Mica was freshly cleaved from 12 mm discs obtained from ProSciTech (Australia), and used immediately. Before use, all glass surfaces were cleaned by soaking for an hour sequentially in 10% Ajax detergent, then 10% nitric acid, and finally 10% sodium hydroxide, each step being followed by rinsing with copious amounts of deionised water. Pentan-1-ol (99.5%) was from Fluka and used as received. 1-decanethiol (96%) was obtained from Aldrich and used as received. The microemulsion used as a structuring phase was formulated using tetradecane (2 wt.%) as the oil phase, SDS (5.5 wt.%) as the surfactant, and pentanol (5.5 wt.%) as a cosurfactant, in water. Ludox HS-30 was obtained from Aldrich as a 30 wt.% dispersion in water and used as received.

2.2 AFM measurements

Rectangular silicon AFM cantilevers ($450 \times 50 \times 2$ μm^3) were custom-fabricated *via* nanolithography, and included a circular gold disc (diameter 45 μm) added ≈ 5 μm from the end by ion deposition.[24,25] This allowed the contact area of the droplets on the cantilever to be precisely known. This area was rendered hydrophobic by reaction with 1 mM decanethiol in absolute ethanol for 20 min. Cantilever spring constants, K, were determined by the method of Hutter and Bechhoeffer,[26] and were in the range 0.1–0.13 N m^{-1} for the cantilevers used in these experiments. The AFM measurements were performed on an Asylum MFP-3D AFM, equipped with a linear variable differential transformer (LVDT) sensor in the Z-movement direction, to allow direct detection of the cantilever Z-position during force measurements. This has been shown to be vital for accurate force-displacement measurements, as instantaneous piezo velocity is non-linear.[24]

Droplet radii were measured microscopically (Nikon Ti2000), Debye lengths were calculated from solution compositions (taking the degree of ionization of SDS to be 0.27, from the work of Bales[27]), and literature values for the surface potentials for silica and mica

were used.[28] Because the effective electrolyte concentration from dissociated SDS was relatively high, the contribution to the pressure between interacting surfaces from electrical double-layer interactions was sufficiently short-range to be completely masked by the contribution from the structural interaction. The contribution to the interaction from the Van der Waals force was calculated using a full retarded Hamaker function, obtained by the method of Lifshitz,[29] but this was also short-range, and hence masked by the presence of the structural pressure.

Measurements using silica particle probes were made using V-shaped cantilevers (MLCT, Veeco probes, spring constant 0.03–0.05 N m^{-1}). The end of the cantilever was brought down into a small amount of epoxy (Araldite Rapid) and this was used to pick up a silica bead of radius 10 μm (Thermo Particle Size Standards). The glue was left to dry for 24 h before the cantilever was used.

Tetradecane droplets were generated by nebulising the oil with a glass syringe over a surface composed of 100 nm thick gold which had been deposited onto a glass cover slip (Menzel-Gläser 22 × 22 mm, #1 thickness) using an Emitech K575x sputter coater, with an intermediate layer of 10 nm of chromium as an adhesion promoter. Before use, the gold surface was partially hydrophobised by immersion in a 1 mM solution of 1-decanethiol/1-mercapto-1-decanol in ethanol for several hours, as described previously.[30] SDS solutions used in conjunction with tetradecane droplets were pre-saturated with tetradecane for 24 h prior to use. PFO droplets were generated by gently discharging a glass syringe of the oil under water to give a coarse emulsion with a range of droplet sizes. The substrate used was a glass Petri dish which had been boiled for 3 h in absolute ethanol,[31] generating a slightly hydrophobic surface suitable for anchoring of droplets (water contact angle 40 degrees). The volume of water added initially was 4 ml. A suitably sized oil droplet was then picked up on the AFM cantilever, and the solution adjusted by addition of 4 ml of concentrated surfactant solution or a microemulsion to the desired concentration, giving a total liquid volume of 8 ml. After equilibration, interactions were measured between the droplet on the cantilever and either another droplet immobilised on the surface, or a flat mica surface. Video microscopy was used to measure droplet sizes, with an accuracy of ±2μm. The AFM setup was scrupulously cleaned between experiments to ensure no surfactant or other contaminant remained.

AFM data were recorded as photodiode voltage *vs.* LVDT displacement. The voltage was converted into a deflection in nanometres by mutliplying by the inverse optical-lever sensitivity, which was determined by measuring the deflection of the cantilever against a rigid surface. The deflection was then converted to force by multiplying by the spring constant. As a consequence of the inherent noise due to thermal fluctuations and scattering of the AFM laser, data were binned by a moving average method, whereby the force value for each separation was averaged with 5 points on each side. Due to the large number of data points acquired, this smoothing was not found to distort the features of the data, but effectively reduced the noise.

2.3 Interfacial Tension Measurements

The interfacial tensions for PFO-SDS solutions, PFO-microemulsion and tetradecane-SDS solution systems were measured using the pendant drop method, utilizing a Dataphysics OCA tensiometer. A pendant drop of oil was generated in solution and allowed to equilibrate for 20 min. After this time, it was photographed, and the profile of the drop perimeter fitted to the Young-Laplace equation using the proprietary instrument software, providing the interfacial tension. These values were found to be 15 ± 2 mN m^{-1} for PFO-SDS (400 mM), 15 ± 2 mN m^{-1} for PFO-SDS (240 mM), and 11 ± 2 mN m^{-1} for PFO-microemulsion. The interfacial tension for the tetradecane-solution interface over the range of SDS concentrations used was 4 ± 2 mN m^{-1}, except where addition of significant amounts of NaCl caused additional surfactant adsorption resulting in a small decrease of interfacial tension to 3.8 ± 2 mN/m. The tetradecane-solution interfacial tension in the presence of 3.5 wt.% Ludox silica particles was measured as 38 ± 2 mN/m. All interfacial tensions were measured at 22 °C.

2.4 SANS measurements

Neutron scattering experiments were carried out on the D22 small-angle diffractometer at the Institut Laue-Langevin, Grenoble, France. A neutron wavelength of $\lambda = 10$ Å with a spread of 9% and two sample-detector positions of 1.4 and 14 m were used with a detector offset to provide a Q range of 0.003–0.387 $Å^{-1}$. Samples were run at a temperature of 20° C. Absolute intensities for $I(Q)$ (cm^{-1}) were determined to within 5% by measuring the incoherent scattering from 1 mm of H_2O. Samples were prepared in Hellma quartz cells with a path-length of 2 mm. Raw SANS data were normalized by subtracting the scattering of the empty cell and a D_2O solvent background. Model fits to the neutron data were generated using the FISH program[32] to iterate a least-squares best fit between experimental data points and predictions of the equations below by changing unconstrained variables.

For a system of ellipsoidal micelles in solution, the scattered intensity, $I(Q)$, as a function of the magnitude of the wave vector, Q, can be expressed as a function of the number of scatterers, N_P, their form factor, $P(Q)$, and the orientationally-averaged structure factor, $S'(Q)$, which accounts for the interactions between scatterers:[33]

$$I(Q) = N_P P(Q) S'(Q) + B \quad (1)$$

where B is a contribution from incoherent background scattering. The form factor for prolate ellipsoids can be expressed as:

$$P(Q) = \int_0^1 \Phi^2(u)\, du \quad (2)$$

where the function $\Phi(u)$ is defined as:

$$\Phi(u) = v(\rho_m - \rho_s)\, \frac{3[\sin(u) - u\cos(u)]}{u^3} \quad (3)$$

In eqn (3), v is the volume of a micelle, and ρ_m and ρ_s are the scattering length densities of the micelle and solvent respectively. The factor u is defined as:

$$u = Q[a^2\mu^2 + b^2(1 - \mu^2)]^{1/2} \quad (4)$$

where a and b are the semi-major and semi-minor axes of the ellipsoid, and μ is the angle subtended by the direction of a and

the wave vector Q. To fit the microemulsion, the axial ratio was set to unity. The orientationally-averaged structure factor is approximated from the centre-to-centre structure factor for isotropic scatterers, $S(Q)$, by the expression:

$$S'(Q) = 1 + \frac{P(Q)^2}{\left\langle |P(Q)|^2 \right\rangle}(S(Q) - 1) \quad (5)$$

where angle brackets denote the angular average of the form factor. To fit the SANS data in these experiments, a Hayter-Penfold screened Coulomb potential for interacting charged spheres was used for $S(Q)$.[34]

2.5 Modelling force-separation behaviour for deformable systems

In order to predict the force of interaction between two droplets, or between a droplet and a plate in the presence of structuring colloids, a procedure developed previously was used.[19] In this method, the force between a solid sphere and plate in the same colloidal solution is used to determine the disjoining pressure due to the effects of colloidal structuring. This disjoining pressure is then used to predict the effect on deformable interfaces.

By employing the Derjaguin approximation,[35] the equivalent interaction free energy per unit area between two parallel plates can be derived from the measured force between a solid particle and a flat plate, by dividing by $2\pi R$ (R being the radius of the solid probe particle). Differentiating this provides the effective disjoining pressure between flat plates. By using this as an input into the Chan-Dagastine-White model,[36,37] it is possible to predict the effect of structural forces on interactions between a droplet and a flat surface, or between two droplets.[19] This model, which calculates the force between a droplet and flat plate, or between two droplets, accounting for their deformation in response to surface forces, has been presented and reviewed in considerable detail,[36,38–40] and hence will not be replicated here.

3 Results and discussion

3.1 Solid systems

In order to fully understand the effect of structural forces on deformable interfaces, AFM measurements were first made of structuring colloids confined between solid surfaces. This allows the effect of structuring in the film to be observed without the complex convolution with the deformability that occurs with droplets. In this geometry, measurements were made between a silica probe particle (of radius 10 μm) and a silica plate, where the structuring phase was comprised of SDS micelles, microemulsion droplets or silica nanoparticles (Fig. 1).

The solid lines in Fig. 1 are fits to the data using a semi-empirical equation that has been shown to provide a close approximation of many structural force profiles for solid systems:[10]

$$\frac{F}{R} = 2\pi A \exp\left(\frac{-h}{\xi}\right) \cos\left(\frac{2\pi h}{\lambda_{\mathrm{AFM}}} + \phi\right) + c \quad (6)$$

where F is the interaction force, R is the radius of the probe particle, A is the oscillation amplitude, h is the separation between solid interfaces, ξ is a correlation length (which determines how rapidly the oscillations decay), λ_{AFM} is the characteristic period (wavelength) of oscillation, ϕ is a phase factor and c is an offset. It is clear from Fig. 1 that the period of oscillation seen between surfaces when colloids are confined in the film is significantly larger than the average hard-sphere diameter of the colloids themselves. It should also be noted that data at separations closer than the maximum of the first oscillation were not included in the fit. This is because the effects of electrical double-layer and Van der Waals forces come into play at these ranges, in addition to the possibility of steric forces from surface-adsorbed surfactant, each of which could potentially distort the oscillatory profile in the final few nanometres before contact.

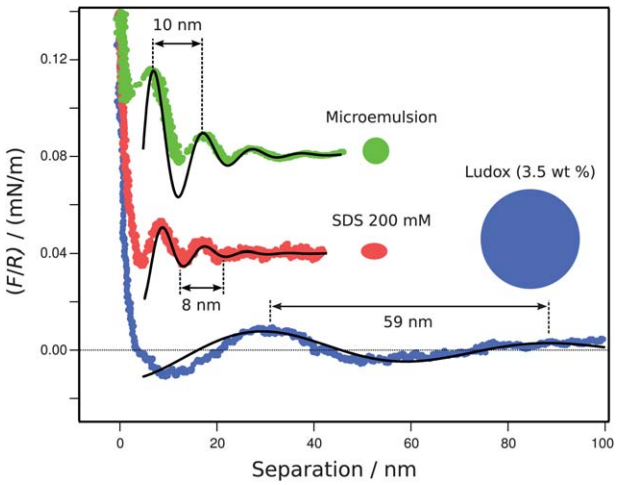

Fig. 1 Force *versus* separation data obtained with the AFM, showing oscillatory structural forces between a silica particle (radius 10 μm) and a silica surface, where the structuring colloids are SDS micelles (effective radius, $R_{\mathrm{eff}} = 1.9$ nm), microemulsion droplets ($R_{\mathrm{eff}} = 2.2$ nm) and Ludox silica particles ($R_{\mathrm{eff}} = 10$ nm). Symbols are AFM data, and solid lines are fits using the semi-empirical equation described in the text (eqn (6)). The hard-sphere/ellipse size of the colloidal additives are shown schematically next to the data sets, relative to the x-axis scale. For the microemulsion and SDS micelle, these are determined from SANS fitting, as described in the text. For the Ludox silica particles, it is the average size as provided by the manufacturer's specification.

3.2 Deformable systems - effect of colloid size and concentration

Interactions were measured using the AFM between a deformable droplet of tetradecane (radius 40 μm) and a mica surface in a 3.5 wt. % dispersion of Ludox silica particles (radius 10 nm), (Fig. 2). The measured force, F, is plotted as a function of the separation, ΔX, between the free end of the cantilever and the mica surface. It can be seen in Fig. 2 that there is no significant difference between the approach and retract branches showing that the film changed its thickness smoothly as a function of cantilever/surface separation. This behaviour is correctly predicted by the Chan-Dagastine-White model, when the structural disjoining pressure (obtained from solid-solid interactions in the same nanoparticle solution, such as that given in Fig. 1) is included. The model prediction is shown as the solid line in Fig. 2. The model also predicts that in this case, the final layer of

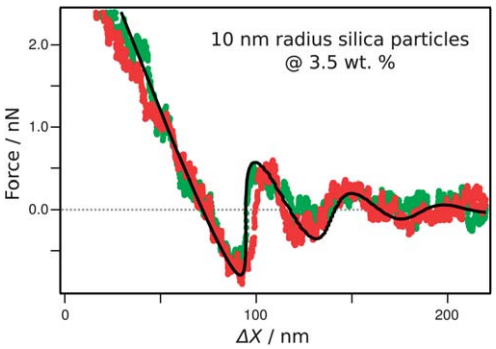

Fig. 2 Interaction force between a tetradecane droplet (radius 40 μm) and a mica surface in a 3.5 wt. % dispersion of silica particles (10 nm radius). Symbols are experimental AFM data for approach (green) and retract (red), and the line is a fit using the Chan-Dagastine-White model with the structural disjoining pressure from the rigid case used as an input. It is noted that no hysteresis is observed between approaching and retracting force curves.

nanoparticles is excluded, and hence the droplet experiences a repulsion at close separations due to electrical double-layer forces between the charged solid-water and oil–water interfaces. In this case, the pressure required to exlude the final layer of nanoparticles is lower than the Laplace pressure within the tetradecane droplet, and hence the droplet remains sufficiently rigid that it can thin the liquid film so as to exclude the final layer of nanoparticles.

When moving to much smaller structuring colloids (SDS micelles of <2 nm radius), the behaviour is significantly different. The force between a tetradecane droplet and mica surface, and between two tetradecane droplets in 150 and 200 mM SDS is shown in Fig. 3. Here, a significant difference is evident in all cases between the approach and retract force curves, where a strong hysteresis is seen. Interestingly, the jumps on both approach and retract occur at larger force magnitudes for the lower concentration, which appears initially counterintuitive. However, the reason appears to be that for the 150 mM case, an extra layer of colloid is squeezed out, leaving two layers remaining between the droplet and surface (or two drops), whereas for 200 mM SDS, three layers remain. This difference is due to an increased pressure barrier encountered at the third layer in the system with the higher concentration of micelles, which favours expansion of the interaction area rather than closer approach of interfaces. This behaviour is clearly dependent on the deformability of the droplets, and would not be seen in rigid systems. In both droplet-plate and droplet-droplet configurations, for 150 mM SDS, the experimental pull-off minima are shallower than predicted by theoretical modeling, despite the position of the jump-in on approach being accurately predicted. This could be due to the slight lack of fidelity in the theoretical representation of the oscillatory force curves between rigid surfaces that are used as an input to the model calculation for the deformable case.

3.3 Deformable systems – effect of curvature and deformability on thin film stability

By analysing more structural systems, it has been possible to explore the effects of size, concentration and interactions

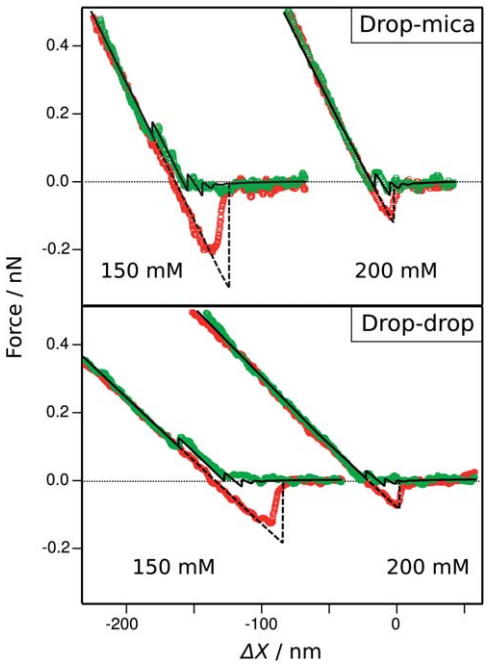

Fig. 3 Interaction forces between a tetradecane droplet (radius 40 μm) and a mica surface (top panel) and between two tetradecane droplets in an aqueous SDS solution at two different concentrations (bottom panel). Symbols are experimental AFM data for approach (green) and retract (red), and the line is a fit using the Chan-Dagastine-White model with the structural disjoining pressure from the rigid case used as an input, showing approach (solid) and retract (dashed) branches. These model fits are presented as 'net' or 'observable' predictions, discussed in section 3.3 below.

between the structuring colloids in considerably more detail than was previously possible. Examples of the predicted force *vs.* separation behaviour between a 40 μm radius tetradecane droplet and a flat plate, using the pressure derived from particle-plate measurements are shown in Fig. 4 for a system of 10 nm radius silica particles (panels A–C) and 150 mM SDS, where the micelles have an effective radius of 1.9 nm (panels D–I). The same data is displayed in panels D–F as in G–I, but in the latter case, instabilities or 'jumps'[19,23] due to deformation of the droplet (shown as arrows in panels D–F) have been taken into account to give the 'observable' force curves that would be obtained in real experiments. It is these observable curves that are shown later in comparison with measured force data. This modelling is complementary to the experimental data shown in Fig. 2 and 3 above, and is presented to allow more insight into the behaviour of the liquid film captured between deformable interfaces when an oscillatory structural pressure is experienced.

In each case, the calculated model data is displayed in terms of three key parameters - the force, F, displacement between the end of the cantilever and surface, ΔX, and the thickness of the aqueous film between the centre of the droplet and the solid surface, $h(0)$ (which, for the case of two droplets interacting, becomes the central thickness of the aqueous film between the two oil–water interfaces).[39,40] Comparing these different representations is useful as it demonstrates that the behaviour seen is dependent on the technique used to probe it. The data obtained experimentally by AFM measurements is force *vs.* ΔX (panels B,

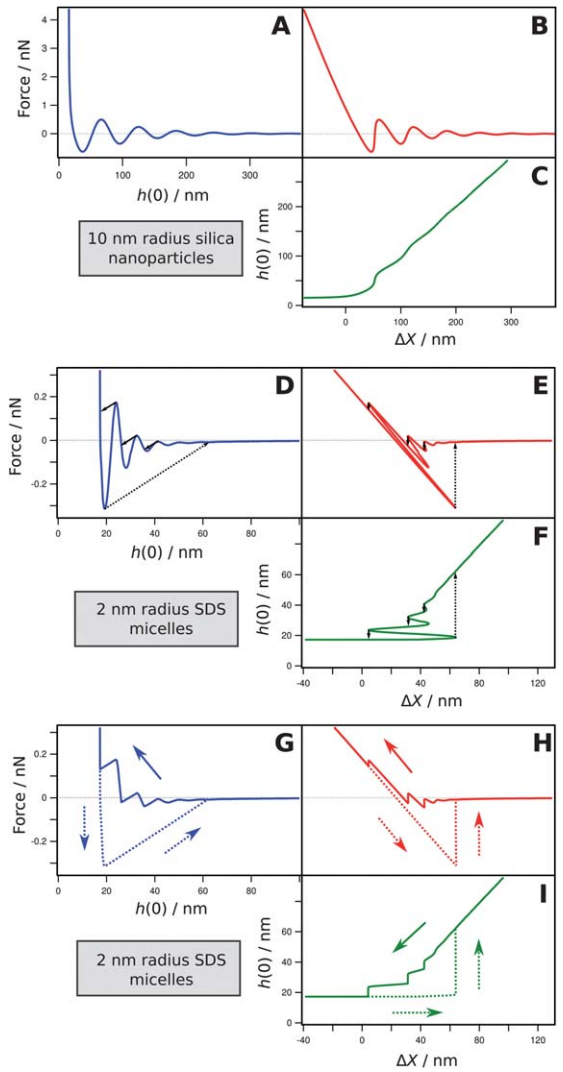

Fig. 4 Theoretical predictions for a tetradecane droplet (radius 40 μm) against a flat surface in a 3.5 wt. % solution of 10 nm radius silica spheres (A–C) and 150 mM SDS solution, where the effective micelle hard-sphere radius is 1.9 nm (D–I). Note the significantly different ranges of the ΔX scale for the two differently sized structuring colloids. In D–F, solid arrows show the expected positions of jump-ins on approach of the droplet towards the surface, caused by film thickness jumping to the next stable value. Dotted arrows show the jump-outs expected on retraction of the droplet from the surface. In G–I, the jump-in and out positions are explicitly accounted for to give 'observable' force curves, showing approach (solid lines) and retract (dotted lines) branches. Here, the arrows show the direction of motion of the droplet.

E,H), and hence this representation is compared with the obtained AFM data.

For the case of large silica particles, the model predicts no hysteretic behaviour in the force *vs.* ΔX relationship. The reason for this is that the long-wavelength oscillations induced by the large particles never cause sufficiently large gradients in the force *vs.* ΔX curve (panel B) to induce mechanical instabilities in the deformable droplet/cantilever system. This is particularly evident in panel C, where the central film thickness is plotted as a function of ΔX. The film only has one equilibrium thickness for any given separation between cantilever and surface, and hence never becomes unstable. These predictions are confirmed by the experimental data shown in Fig. 2.

As seen in Fig. 3, when SDS micelles, which are significantly smaller, are used as the structuring colloid, the behaviour changes dramatically. This is also predicted by the model (panels D–F). The gradient of the force *vs.* ΔX curve (panel E) reverses its sign in several places, giving multiple possible equilibrium force values for a given separation. At these points, the coupled system of the cantilever and deformable droplet become unstable, and 'jump' to the next stable force–distance position.[19,23] This behaviour is particularly clear when the film thickness is plotted as a function of ΔX, in panel F. As the cantilever approaches the surface, the film between the droplet and surface thins, initially linearly at large separations. When structural forces dominate the disjoining pressure in the film, it jumps to the next stable position, as ΔX changes monotonically during approach. On retract, the instability occurs at a different ΔX value, as the film is 'trapped' at a certain thickness by the attractive well of the structural oscillation. The net result of this behaviour is that the measured force curve looks distinctly different on approach than on retract, as seen in panels G–I. Interestingly, the 'net' force curve obtained in panel G is very similar to those seen for structure-forming systems when analysed using SFA[13] or film balance techniques[5,14] (which measure the force or pressure as a function of film thickness).

Because the droplet can deform and change its interfacial profile in response to surface forces, the force *vs.* separation behaviour seen will clearly be a function of the drop's radius and interfacial tension, which in concert control its Laplace pressure, by the Young-Laplace equation ($\Delta p = 2\gamma/R$, where Δp is the pressure difference between the oil droplet and solution, γ is the interfacial tension and R is the droplet radius). Hence, a smaller droplet is much more rigid, and a larger droplet more deformable.[40] By using the model to assess the predicted structural forces experienced by different droplet sizes, the effect of this size-dependent deformability is seen (Fig. 5, top panel).

For a 1 μm droplet, the intrinsic Laplace pressure is sufficiently high that it behaves much like a rigid particle,[41] and hence there is little deformation of the interface. This results in a prediction that there will be no hysteresis in the approach and retract force *vs.* distance behaviour. It is also predicted that the last layer of micelles is not excluded, but would experience some compression. This could be an artefact due short-range surface interaction effects from the solid particle-probe data which was used as input in generating these model data. It is difficult to say whether such a compression would be seen experimentally. At this droplet size and for these conditions, the attractive minima are very shallow and small in magnitude. At a radius of 10 μm, the force curve begins to show hysteresis, as the film thickness jumps between stable values on approach and retract. Also in this case, one layer of micelles remains between the droplet and surface, regardless of the applied force, as the pressure required to exclude it is greater than the Laplace pressure of the droplet. Hence, the droplet will continue to deform and flatten in preference to squeezing out the final layer of micelles. By increasing the droplet radius a further order of magnitude to 100 μm, the hysteresis becomes much more pronounced, and a significantly larger attractive force well is experienced on retraction. Because the Laplace pressure of the droplet is much lower again, here two

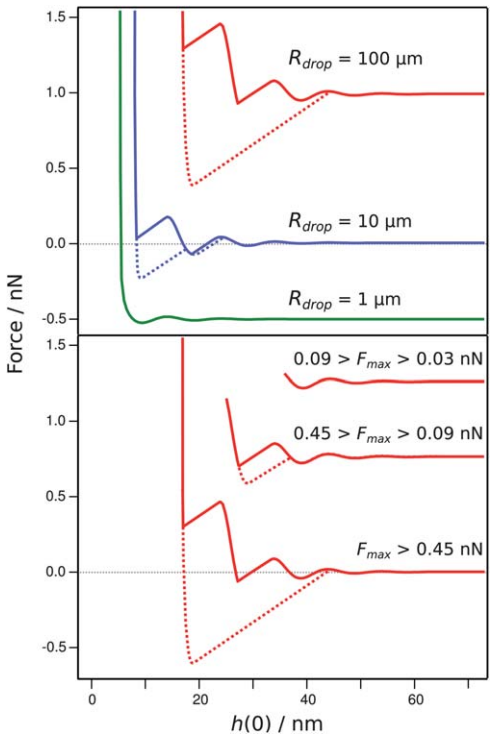

Fig. 5 Top panel: the effect of droplet size on the predicted structural forces observed between two droplets interacting in 200 mM SDS solution. Observable force curves accounting for jumps due to film instabilities are presented (see Fig. 4 D–I). All parameters other than radius are kept constant: interfacial tension, $\gamma = 15$ mN m^{-1}), contact angle, $\theta = 150°$, surface potential, $\Phi = -40$ mV and ionic strength, $I = 0.05$ M. Bottom panel: the effect of the maximum force experienced (F_{max}) during approach on the force hysteresis obtained for interactions between two droplets of 100 μm radius. Parameters are as above.

layers of micelles would be predicted to remain between the droplet and surface. Evidently, a similar series of changes could be obtained by a systematic change in interfacial tension, such as could be achieved by changing the concentration or interfacial affinity of stabilisers.

It is clear from model predictions that the force behaviour seen is dependent also on the maximum force which is applied or attained. For free emulsion droplets interacting in a shear flow or *via* Brownian motion, this force is also linked to their size and interfacial tension. This is demonstrated in Fig. 5, bottom panel. For the 100 μm droplet shown, different force minima can be accessed by approaching until different maximum force values (F_{max}) are reached. This suggests that the flocculation pathway that is available to droplets is also dependent on the maximum force or energy with which they are able to interact, leading to the possibility of shear-dependent behaviour. Depending on their collision histories, pairs of droplets may be expected to experience different average separations, controlled by the particular minimum they are 'trapped' in. Such 'ratchet' force curves result in a discretised and history-dependent diffusion behaviour, which could be further explored with techniques such as TIRM.[7,42]

In this work, our previous paper[19] and the work of Gromer *et al.*,[21] hysteresis is observed in the approach and retract force curves between deformable interfaces in the presence of nanocolloids at concentrations that induce structural forces. Interestingly, in the study by Zeng *et al.* on the force between a deformable air bubble (radius 400 μm) and a silica particle (radius 3.5 μm) in the presence of nanoparticles, such hysteresis is not observed.[22] Based on the above data and discussion, this is most likely due to the relatively large size of the nanoparticles employed. Here, we have shown through theoretical modelling (in agreement with experimental evidence) that the nature and overall effects of structural forces between deformable interfaces can be controlled by the size of the structuring colloid, the interfacial tension of the interfaces, their radii of curvature and the force with which bodies interact. Hysteresis may or may not occur depending on these factors.

3.4 Correlation of bulk colloid structure with structure in thin films

In order to further explore the relationship between the bulk structuring of the colloidal phases and how this relates to their influence on forces in thin films, small-angle neutron scattering (SANS) was used to analyse bulk samples of the structuring colloids. SANS has grown to prominence as the tool of choice for analysing soft matter systems,[43] where its non-destructive and versatile nature is particularly suited to probing length-scales typical of micelles and microemulsion droplets.[44] By utilising the significant difference in the scattering length of hydrogen and deuterium, isotopic substitution can be used to highlight specific structures, interfaces, or phases.[45] In these experiments, hydrogenated SDS was prepared in deuterated water (D_2O) in order to provide strong contrast from the hydrocarbon core of the micelles. By fitting mathematical predictions of scattering for the systems (as described in the methods section), it was possible to extract information on the micelle size and hence aggregation number, average inter-micelle distance and charge.

There has been considerable debate in the literature about the precise shape of SDS micelles at various concentrations and salt conditions, with different authors suggesting the same samples are rough spheres,[46] oblate ellipsoids[47,48] and discs.[49] In these experiments, best fits to the SANS data were achieved with an oblate ellipsoidal form factor,[33] coupled with a Hayter-Penfold structure factor[34] to account for the interactions between the charged micelles. SANS data and model fits for SDS at various concentrations are shown in Fig. 6.

As a consistency check, scattering data was obtained for a sample of 200 mM SDS that had been equilibrated with an excess tetradecane phase overnight, shown as the inset to Fig. 6 (note that the two plots have been vertically offset for clarity). This was to demonstrate that no significant difference in the size of micelles was observed due to the presence of tetradecane, as would be expected, as SDS cannot make a three-component microemulsion with tetradecane and water. In fact, there is virtually no difference in the scattering from SDS micelles before and after equilibration with tetradecane (as shown by the fitting parameters, given in Table 1), suggesting that the micelles are unable to host a significant number of tetradecane molecules. This result is important as it allows direct comparison between the various data sets in this and previous experiments.[19]

It can be seen that the intensity of the scattering data increases with SDS concentration, and hence volume fraction of micelles,

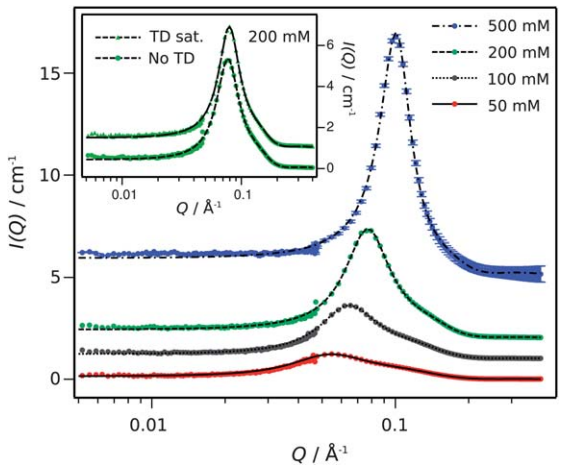

Fig. 6 Small-angle neutron scattering data for SDS micellar solutions at various concentrations. Symbols are experimental scattering data, and lines are fits generated as described in the text. Data sets are vertically offset for clarity. Example error bars are shown for the 500 mM case. The inset shows the effect of pre-saturating the 200 mM solution with tetradecane.

as would be expected. The position of the characteristic peak in the SANS data, Q_{max}, due to the strong structure factor from interactions between the charged micelles, provides an indication of the average inter-micelle spacing, λ_{SANS}, by the relationship $\lambda_{SANS} = 2\pi/Q_{max}$.[10] This clearly decreases with increasing micelle number concentration. Structure factors for the SDS concentrations used in these experiments are shown in Fig. 7.

Parameters obtained by model fitting of the SANS data are provided in Table 1. To obtain the fits, the semi-minor axis of the prolate ellipsoid was fixed at 1.67 nm, the length of a fully extended dodecyl hydrocarbon chain,[50] and the axial ratio, r, was used as a fitting parameter. The effective sphere radius of the micelles, assuming constant volume, R_{eff} was therefore obtained as $R_{eff} = (1.67^3 r)^{1/3}$ nm. Aggregation numbers were calculated by dividing the micellar volume by the molecular volume of the hydrocarbon chain (351 Å^3).[49,50] This analysis assumes that the core is smooth and composed entirely of the hydrocarbon portions of SDS molecules, without penetration of any water. The number concentration of micelles, c_m, was obtained by dividing the concentration of SDS (minus the CMC) by the aggregation number. The fractional charge, β, was calculated by dividing the micelle aggregation number by the number of charges per micelle, z.

Derived values of the micelle size, aggregation number and charge are in good agreement with literature values from previous studies, including those with quite different analyses.[33,46,47] As expected, the average inter-micelle distance obtained from the fitted structure factors, $\lambda_{SANS} = 2\pi/Q_{max}$, scales inversely with the number concentration of micelles, as in a given volume, an increase in the absolute number of micelles must bring them, on average closer together.

Addition of tetradecane and a cosurfactant (pentanol) to the SDS micelles allowed thermodynamically stable microemulsion droplets to be generated.[51] SANS of these droplets showed that the hydrocarbon cores (composed of tetradecane and the hydrocarbon chains of SDS and pentanol) had swollen to a radius of 2.2 nm. Measuring the structural forces between a droplet and plate or between two droplets in this case was performed using perfluorooctane as the phase of the large, confining droplets. This fluorinated oil is immiscible with

Table 1 Parameters obtained from model fitting of SANS data, and from AFM experiments. From SANS fits, r is the axial ratio for prolate ellipses, R_{eff} is the effective sphere radius, N_{agg} is the number of monomers aggregated in each micelle, c_m is the number concentration of micelles, β is the fractional charge of the micelles and λ_{SANS} is the average inter-micellar spacing determined from the structure factor. From AFM experiments between rigid interfaces, λ_{AFM} is the characteristic period (wavelength) of oscillation

Sample	r	R_{eff}/ nm	N_{agg}	c_m/ mM	β	λ_{SANS}/ nm	λ_{AFM}/ nm
SDS: 50 mM	1.37	1.84	75	0.57	0.21	10.8	—
100 mM	1.50	1.89	80	1.15	0.23	9.5	—
150 mM	—	—	—	—	—	(8.7)[a]	9.6
200 mM	1.65	1.96	90	2.14	0.24	7.9	—
200 mM (tetradecane sat.)	1.68	1.97	91	2.09	0.25	7.9	8.8
200 mM, 10 mM NaCl	1.74	2.00	95	2.03	0.24	7.7	8.7
200 mM, 50 mM NaCl	1.95	2.07	106	1.81	0.23	7.2	8.5
240 mM	—	—	—	—	—	(7.6)[a]	8.7[b]
400 mM	—	—	—	—	—	(6.5)[a]	8.0[b]
500 mM	1.84	2.03	100	4.91	0.21	6.0	—
Microemulsion	1.00[c]	2.20	(127)[d]	(1.45)[e]	0.27	8.0	9.0

[a] Extrapolated from fitted values of λ_{SANS}. [b] From ref. 19. [c] For the microemulsion, it was assumed that droplets would be spherical, and hence the axial ratio was fixed at 1, and the radius was not fixed at 1.67 nm, but allowed to be fitted as a free parameter. [d] As the microemulsion droplets are composed of both SDS and pentanol, this value based only on the core volume occupied by SDS is expected to be an overestimate. Penetration of pentanol hydrocarbon chains into the micellar core would act to reduce this number, although the effect is hard to quantify. [e] This value is calculated from the SDS aggregation number, and hence is likely to be an underestimate, for the same reasons given in[a].

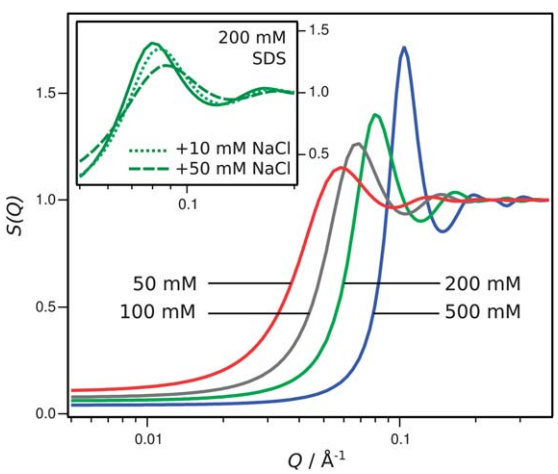

Fig. 7 Structure factors, $S(Q)$, from model fits to SANS data for the SDS concentrations shown in Fig. 6. The peak in the structure factor is used to determine the average inter-micelle spacing. The inset shows the effect of added electrolyte on the 200 mM SDS sample.

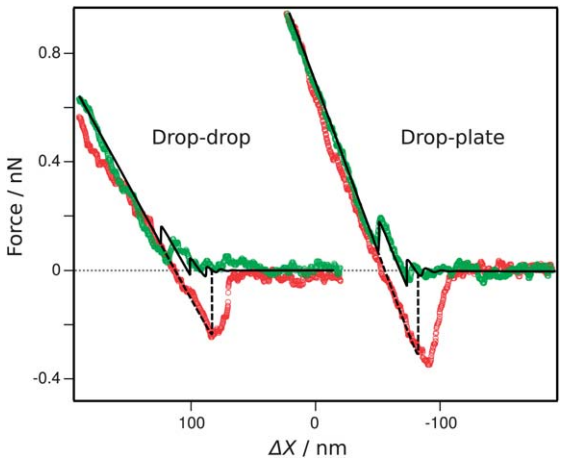

Fig. 8 Interaction force between a PFO droplet (radius 45 μm) and a mica surface and between two PFO drops. Symbols are experimental AFM data for approach (green) and retract (red), and the line is a fit using the Chan-Dagastine-White model with the structural disjoining pressure from the rigid case used as an input, showing approach (solid) and retract (dashed) branches.

tetradecane, and so could not be dissolved into the microemulsion droplets.[52] Such interactions are shown in Fig. 8.

It is seen that there is little difference between the form of the force behaviour when comparing microemulsion droplets and micelles. This raises an interesting point about the nature of the structuring colloid: micelles are dynamic on a microsecond timescale, capable of exchanging monomers with the bulk solution, and also capable of entirely breaking down (where a micelle composed of *n* surfactant molecules spontaneously disassembles into *n* free monomers). Microemulsion droplets may exchange surfactant and cosurfactant monomers, but do not have a thermodynamically accessible breakdown pathway. Hence, it is posited that the structuring effects seen on confinement are, as expected, due to depletion-like interactions controlled by effective differences in osmotic pressure, and that no dynamic effects are seen in the film.

3.5 Deformable systems – effect of salt

One of the significant questions which remains concerning structural forces is whether the behaviour in the film during close approach of surfaces is reflective of bulk structure of the colloids, or whether the act of confinement induces or changes structure. To probe this further, AFM and SANS measurements were made on samples with 200 mM SDS and varying concentrations of added salt. As expected, the addition of salt encourages slightly larger micelles to form, due to decreased repulsions between the charged headgroups of the surfactant monomers. This therefore changes the number density of micelles, and their average spacing slightly. However, such variations are relatively small (Table 1), as seen when comparing the structure factors on addition of salt (inset to Fig. 7). Scattering intensity data from these studies are shown in Fig. 9.

If structural interactions in thin films are reflective solely of the bulk inter-colloid separation, it would be expected that little difference would be seen for interactions between systems when only salt is changed. This indeed appears to be the case for solid systems, where the characteristic period (see Table 1) only shows a slight dependence on salt. There appears to be a close correlation between the average inter-micelle distance, λ_{SANS}, from fitting the SANS structure factor and that from AFM measurements, λ_{AFM}, between a particle and plate, with an approximately constant, small discrepancy. This could be indicative of a 'wall effect,' due possibly to interactions between the micelles and the solid surfaces. In contrast to conventional understanding, it has recently been shown that despite the negative charges on both SDS and the silica surfaces, a significant amount of SDS adsorption may occur at silica surfaces.[53,54] This may be expected to affect the final few oscillations at closest approach. Because the amplitude of oscillation decays rapidly with increasing separation, it is only the first 1–2 oscillations which can be reliably fitted. An alternative explanation is that when the structuring colloids are confined between approaching surfaces, they have less freedom of movement because of interactions with the surface, which could cause an effective increase in their average spacing when compared to the bulk.

When moving to a deformable system, the change in behaviour on addition of salt is significantly more marked (Fig. 10). Here, the interactions between two tetradecane droplets in 200 mM SDS at three salt conditions are plotted. The behaviour can be predicted by modelling using the disjoining pressures derived from the interaction forces measured between a solid particle and solid surface, which suggests that droplets offer a much more sensitive probe to these subtle effects than solid spheres, as they are able to deform and increase their effective area of interaction. This amplifies the effects of small differences in disjoining pressure, allowing them to be detected more readily. From Fig. 10, it can be seen that the addition of 10 mM NaCl has only a minor effect on the forces seen, whereas addition of 50 mM salt increases the magnitude of the forces experienced on jump-in and jump-out significantly. This is due to an extra layer of micelles being excluded for the 50 mM case, which did not occur at the other salt conditions. This is clearly due to the deformability of the droplet, which allows it to act as an adaptable probe. Significantly, on addition of salt, deformability is still able to prevent coalescence between pairs of droplets, although the

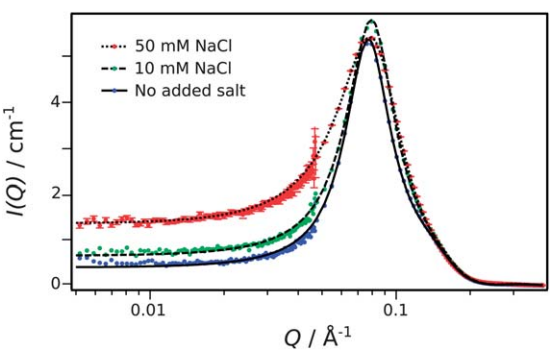

Fig. 9 SANS intensity data for 200 mM SDS concentration, showing the effect of added salt. Symbols are experimental scattering data, and lines are fits generated as described in the text. Example error bars are shown for the uppermost data set.

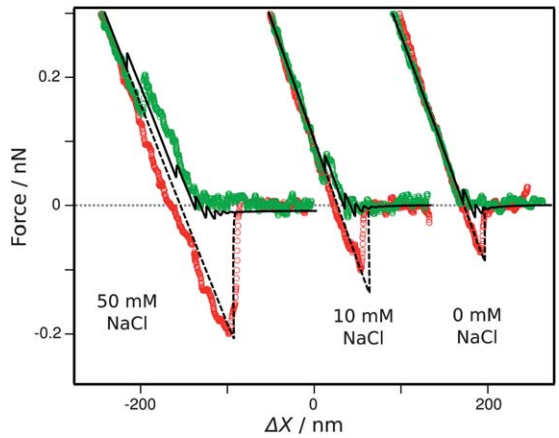

Fig. 10 Interaction force between two tetradecane droplets in 200 mM SDS, showing the effect of added salt. Symbols are experimental AFM data for approach (green) and retract (red), and the line is a fit using the Chan-Dagastine-White model with the structural disjoining pressure from the rigid case used as an input, showing approach (solid) and retract (dashed) branches.

strength of depletion flocculation that they experience is enhanced substantially.

4 Summary and conclusions

Oscillatory structural forces were measured between the deformable interfaces of emulsion oil droplets, using the atomic force microscope. These oscillations were induced by the presence of SDS micelles, microemulsion droplets or silica nanoparticles, between micrometre-scale tetradecane or perfluorooctane droplets in close proximity. Measured forces between rigid surfaces were used to construct the structural component of the disjoining pressure between flat plates, and this component was used in the Chan-Dagastine-White model to predict the force between pairs of deformable droplets, and between droplets and solid surfaces. Close agreement was seen between these model predictions and data directly obtained between such deformable interfaces in the presence of structuring colloids. Comparison with small-angle neutron scattering measurements of the bulk structure of the colloidal additives suggests that the structure in the film does not differ significantly from that in the bulk.

A number of new observations have emerged that are specific to deformable interfaces. Specifically, the presence and absence of hysteresis (direction-dependence) in the force *vs.* separation behaviour for emulsion droplets can be predicted, based on the droplet size/deformability and the size of the colloidal additives. The size of attractive minima (wells) induced by such hysteresis depends on the maximum force that the droplets experience on approach, leading to pressure- and path-dependent attractions. These could be readily determined as the deformable nature of droplets makes them more sensitive probes to subtle changes in the oscillatory pressure profile that arises from structuring of colloidal additives, when compared to rigid surfaces. The potential implications of these findings are that the demonstrated path-dependent attractions may result in shear-dependent flocculation and rheology behaviour for emulsions, where equilibrium inter-droplet distances depend on how the emulsion has been prepared and handled.

Acknowledgements

The subcommittee and the ILL are thanked for the allocation of beam time. X. S. Tang and S. O'Shea are thanked for preparing the cantilevers used. The ARC is thanked for financial support, and the Particulate Fluids Processing Centre, a special research centre of the ARC, provided infrastructure support for the project.

References

1 D. T. Wasan, A. D. Nikolov and F. Aimetti, *Adv. Colloid Interface Sci.*, 2004, **108–109**, 187–195.
2 S. Asakura and F. Oosawa, *J. Chem. Phys.*, 1954, **22**, 1255–1256.
3 J. M. H. M. Scheutjens and G.-J. Fleer, *Adv. Colloid Interface Sci.*, 1982, **16**, 361–380.
4 S. Biggs, R. R. Dagastine and D. C. Prieve, *J. Phys. Chem. B*, 2002, **106**, 11557–11564.
5 A. D. Nikolov and Was, *J. Colloid Interface Sci.*, 1989, **133**, 1–12.
6 C. E. McNamee, Y. Tsujii, H. Ohshima and M. Matsumoto, *Langmuir*, 2004, **20**, 1953–1962.
7 D. L. Sober and J. Y. Walz, *Langmuir*, 1995, **11**, 2352–2356.
8 N. C. Christov, K. D. Danov, Y. Zeng, P. A. Kralchevsky and R. von Klitzing, *Langmuir*, 2010, **26**, 915–923.
9 A. Tulpar, P. R. V. Tassel and J. Y. Walz, *Langmuir*, 2006, **22**, 2876–2883.
10 S. H. L. Klapp, Y. Zeng, D. Qu and R. von Klitzing, *Phys. Rev. Lett.*, 2008, **100**, 118303.
11 M. Piech and J. Y. Walz, *J. Phys. Chem. B*, 2004, **108**, 9177–9188.
12 A. Sharma, S. N. Tan and J. Y. Walz, *J. Colloid Interface Sci.*, 1997, **191**, 236–246.
13 R. G. Horn and J. N. Israelachvili, *J. Chem. Phys.*, 1981, **75**, 1400–1411.
14 V. Bergeron and C. J. Radke, *Langmuir*, 1992, **8**, 3020–3026.
15 R. Roth, R. Evans and S. Dietrich, *Phys. Rev. E: Stat. Phys., Plasmas, Fluids, Relat. Interdiscip. Top.*, 2000, **62**, 5360–5377.
16 B. Fazelabdolabadi, J. Y. Walz and P. R. V. Van Tassel, *J. Phys. Chem. B*, 2009, **113**, 13860–13865.
17 S. Grandner, Y. Zeng, R. von Klitzing and S. H. L. Klapp, *J. Chem. Phys.*, 2009, **131**, 154702.
18 P. A. Kralchevsky, A. D. Nikolov, D. T. Wasan and I. B. Ivanov, *Langmuir*, 1990, **6**, 1180–1189.
19 R. F. Tabor, D. Y. C. Chan, F. Grieser and R. R. Dagastine, *J. Phys. Chem. Lett.*, 2011, **2**, 434–437.
20 V. Bergeron, *J. Phys.: Condens. Matter*, 1999, **11**, R215–238.
21 A. Gromer, R. Penfold, A. P. Gunning, A. R. Kirby and V. J. Morris, *Soft Matter*, 2010, **6**, 3957–3969.
22 Y. Zeng and R. von Klitzing, *Soft Matter*, 2011, **7**, 5329–5338.
23 D. Bhatt, J. Newman and C. J. Radke, *Langmuir*, 2001, **17**, 116–130.
24 O. Manor, I. U. Vakarelski, G. W. Stevens, F. Grieser, R. R. Dagastine and D. Y. C. Chan, *Langmuir*, 2008, **24**, 11533–11543.
25 I. U. Vakarelski, R. Manica, X. Tang, S. J. O'Shea, G. W. Stevens, F. Grieser, R. R. Dagastine and D. Y. C. Chan, *Proc. Natl. Acad. Sci. U. S. A.*, 2010, **107**, 11177–11182.
26 J. L. Hutter and J. Bechhoefer, *Rev. Sci. Instrum.*, 1993, **64**, 1868–1873.
27 B. L. Bales, *J. Phys. Chem. B*, 2001, **105**, 6798–6804.
28 P. J. Scales, F. Grieser and T. W. Healy, *Langmuir*, 1990, **6**, 582–589.
29 I. E. Dzaloshinskii, E. M. Lifshitz and L. P. Pitaerskii, *Adv. Phys.*, 1961, **10**, 165–209.
30 H. E. Lockie, R. Manica, G. W. Stevens, F. Grieser, D. Y. C. Chan and R. R. Dagastine, *Langmuir*, 2011, **27**, 2676–2685.
31 S. Biggs and F. Grieser, *J. Colloid Interface Sci.*, 1994, **165**, 425–430.
32 R. K. Heenan, *Fish Data Analysis Program, RAL-89-129*, Rutherford Appleton Laboratory technical report, 1989.
33 E. Y. Sheu, C.-F. Wu and S.-H. Chen, *J. Phys. Chem.*, 1986, **90**, 4179–4187.
34 J. B. Hayter and J. Penfold, *Colloid Polym. Sci.*, 1983, **261**, 1022–1030.

35 J. N. Israelachvili, *Intermolecular and Surface Forces*, Academic Press, San Diego, 1991.
36 D. Y. C. Chan, R. R. Dagastine and L. R. White, *J. Colloid Interface Sci.*, 2001, **236**, 141–154.
37 R. F. Tabor, D. Y. C. Chan, F. Grieser and R. R. Dagastine, *Angew. Chem., Int. Ed.*, 2011, **50**, 3454–3456.
38 R. R. Dagastine and L. R. White, *J. Colloid Interface Sci.*, 2002, **247**, 310–320.
39 D. Y. C. Chan, R. Manica and E. Klaseboer, *Soft Matter*, 2011, **7**, 2235–2264.
40 D. Y. C. Chan, E. Klaseboer and R. Manica, *Adv. Colloid Interface Sci.*, 2011, **165**, 70–90.
41 R. R. Dagastine, D. C. Prieve and L. R. White, *J. Colloid Interface Sci.*, 2000, **231**, 351–358.
42 S. Biggs, D. C. Prieve and R. R. Dagastine, *Langmuir*, 2005, **21**, 5421–5428.
43 I. Grillo, Small-Angle Neutron Scattering and Applications in Soft Condensed Matter, in *Soft Matter Characterization*, ed. R. Borsali and R. Pecora, Springer, New York, 2008, pp. 723–782.
44 R. F. Tabor, J. Eastoe and I. Grillo, *Soft Matter*, 2009, **5**, 2125–2129.
45 R. F. Tabor, J. Eastoe, P. J. Dowding, I. Grillo and S. E. Rogers, *J. Colloid Interface Sci.*, 2010, **344**, 447–450.
46 J. B. Hayter and J. Penfold, *J. Chem. Soc., Faraday Trans. 1*, 1981, **77**, 1851–1863.
47 S. Bucci, C. Fagotti, V. Degeorgio and R. Piazza, *Langmuir*, 1991, **7**, 824–826.
48 P. A. Hassan, G. Fritz and E. W. Kaler, *J. Colloid Interface Sci.*, 2003, **257**, 154–162.
49 Bergstrom and J. S. Pedersen, *Phys. Chem. Chem. Phys.*, 1999, **1**, 4437–4446.
50 C. Tanford, *J. Phys. Chem.*, 1972, **76**, 3020–3024.
51 M. Almgren, F. Grieser and J. K. Thomas, *J. Am. Chem. Soc.*, 1980, **102**, 3188–3193.
52 R. F. Tabor, S. Gold and J. Eastoe, *Langmuir*, 2006, **22**, 963–968.
53 G. R. Iglesias, W. Wachter, S. Ahualli and O. Glatter, *Soft Matter*, 2011, **7**, 4619–4622.
54 S. Ahualli, G. R. Iglesias, W. Wachter, M. Dulle and O. Glatter, *Langmuir*, 2011, DOI: 10.1021/la201242d.

